

Observation of thermal Hawking radiation and its temperature in an analogue black hole

Juan Ramón Muñoz de Nova¹, Katrine Golubkov¹, Victor I. Kolobov¹ & Jeff Steinhauer^{1*}

The entropy of a black hole¹ and Hawking radiation² should have the same temperature given by the surface gravity, within a numerical factor of the order of unity. In addition, Hawking radiation should have a thermal spectrum, which creates an information paradox^{3,4}. However, the thermality should be limited by greybody factors⁵, at the very least⁶. It has been proposed that the physics of Hawking radiation could be verified in an analogue system⁷, an idea that has been carefully studied and developed theoretically^{8–18}. Classical white-hole analogues have been investigated experimentally^{19–21}, and other analogue systems have been presented^{22,23}. The theoretical works and our long-term study of this subject^{15,24–27} enabled us to observe spontaneous Hawking radiation in an analogue black hole²⁸. The observed correlation spectrum showed thermality at the lowest and highest energies, but the overall spectrum was not of the thermal form, and no temperature could be ascribed to it. Theoretical studies of our observation made predictions about the thermality and Hawking temperature^{29–33}. Here we construct an analogue black hole with improvements compared with our previous setup, such as reduced magnetic field noise, enhanced mechanical and thermal stability and redesigned optics. We find that the correlation spectrum of Hawking radiation agrees well with a thermal spectrum, and its temperature is given by the surface gravity, confirming the predictions of Hawking's theory. The Hawking radiation observed is in the regime of linear dispersion, in analogy with a real black hole, and the radiation inside the black hole is composed of negative-energy partner modes only, as predicted.

Our analogue black hole consists of a flowing Bose–Einstein condensate. The flow velocity v_{out} in the region $x < 0$ is less than the speed of sound c_{out} , as indicated in Fig. 1a. This region corresponds to the outside of a black hole. For $x > 0$, the flow is supersonic ($v_{\text{in}} > c_{\text{in}}$), corresponding to the inside of the black hole. In this region, the sound cones are tilted to the extent that all phonons travel inward, away from the sonic horizon at $x = 0$. In other words, a phonon travelling towards the horizon in the ‘free-falling’ frame (the frame comoving with the flow) travels away from the horizon in the laboratory frame. The phonon is unable to reach the horizon, in analogy with a particle inside a black hole.

For an analogue black hole, the Hawking temperature is given by $\hbar g/2\pi c$ (ref. 7), where the analogue surface gravity for an effectively one-dimensional flow is $g = c(dv/dx - dc/dx)$ (ref. 9), and where the derivatives and speed of sound c are evaluated at the sonic horizon. For a stationary and effectively one-dimensional flow, nv is a constant, where n is the one-dimensional density. We can thus write the Hawking temperature T_{H} as

$$k_{\text{B}}T_{\text{H}} = -\frac{\hbar}{2\pi} \left(\frac{c}{n} \frac{dn}{dx} + \frac{dc}{dx} \right) \Bigg|_{x=0} \quad (1)$$

where k_{B} is Boltzmann's constant. Equation (1) is the predicted temperature of the Hawking radiation in an analogue black hole. We evaluate it using the measured $c(x)$ and $n(x)$. It is derived using a linear dispersion relation, in analogy with massless particles emanating from

a real black hole. In a Bose–Einstein condensate, the dispersion relation is linear in the low-energy limit. Thus, we should create an analogue black hole with sufficiently low Hawking temperature that the radiation is in the linear regime of the dispersion relation. We can then test whether the emitted Hawking radiation obeys the prediction of equation (1). There are several theoretical works suggesting that this should be the case. Using previous analytical results for a system similar to this experiment¹³, we find that equation (1) gives an accurate prediction for $k_{\text{B}}T_{\text{H}} \lesssim 0.14 mc_{\text{out}}^2$, where m is the mass of the atom. We will show that the experiment is within this limit. Parentani and colleagues²⁹ studied our previous experiment²⁸, and concluded that the spectrum should be accurately Planckian, and that the temperature should agree with the relativistic prediction of equation (1) to within 10%. Coutant and Weinfurter³⁰ also studied the previous work and found that the temperature is expected to be close to Hawking's prediction, equation (1).

We test Hawking's prediction by measuring the spectrum of correlations between the Hawking and partner modes, $\langle \hat{b}_{\text{H}} \hat{b}_{\text{p}} \rangle$, where \hat{b}_{H} and \hat{b}_{p} are the annihilation operators for the Hawking and partner modes, respectively. Fortunately, $\langle \hat{b}_{\text{H}} \hat{b}_{\text{p}} \rangle$ is largely free of background correlations. It represents correlations between the inside and outside of the black hole, where Hawking radiation is posited to be the dominant source of such correlations. By contrast, any source of excitations can add to the background of the population $\langle \hat{b}_{\text{H}}^\dagger \hat{b}_{\text{H}} \rangle$. Indeed, the background of $\langle \hat{b}_{\text{H}}^\dagger \hat{b}_{\text{H}} \rangle$ represents the difficulty in observing Hawking radiation from a real black hole. Since we work in the regime of low Hawking temperature and linear dispersion, there is negligible coupling to the mode copropagating with the flow^{12,29}. Thus, we can use the 2×2 Bogoliubov transformation considered by Hawking², $\hat{b}_{\text{H}} = \alpha \hat{b}_{+} + \beta \hat{b}_{-}^{\dagger}$ and $\hat{b}_{\text{p}} = \alpha \hat{b}_{-} + \beta \hat{b}_{+}^{\dagger}$, where \hat{b}_{+} and \hat{b}_{-} are annihilation operators for the positive- and negative-energy incoming modes, respectively, and where $|\alpha|^2 = |\beta|^2 + 1$ and $|\beta|^2 = 1/(e^{\hbar\omega/k_{\text{B}}T_{\text{H}}} - 1)$. This immediately gives $\langle \hat{b}_{\text{H}} \hat{b}_{\text{p}} \rangle = \alpha\beta$ in the vacuum of incoming modes. We can thus compare our measurement of $|\langle \hat{b}_{\text{H}} \hat{b}_{\text{p}} \rangle|^2$ to $(|\beta|^2 + 1)|\beta|^2$, where $|\beta|^2$ is the Planck distribution at the predicted Hawking temperature, equation (1).

The Hawking radiation is observed via the density–density correlation function^{10,11} $G^{(2)}(x, x') = \sqrt{\xi_{\text{out}} \xi_{\text{in}} / n_{\text{out}} n_{\text{in}}} \langle \delta n(x) \delta n(x') \rangle$, where $n_{\text{out(in)}}$ is the density outside (inside) the black hole, $\xi_{\text{out(in)}} = \hbar/mc_{\text{out(in)}}$, and x and x' are in units of the healing length $\xi = \sqrt{\xi_{\text{out}} \xi_{\text{in}}} = 1.8 \mu\text{m}$. We previously found¹⁵ that $\langle \hat{b}_{\text{H}} \hat{b}_{\text{p}} \rangle$ is readily extracted from $G^{(2)}(x, x')$ by the relation

$$S_0 \langle \hat{b}_{\text{H}} \hat{b}_{\text{p}} \rangle = \sqrt{\frac{\xi_{\text{out}} \xi_{\text{in}}}{L_{\text{out}} L_{\text{in}}}} \int dx dx' e^{ik_{\text{H}}x} e^{ik_{\text{p}}x'} G^{(2)}(x, x') \quad (2)$$

where $L_{\text{out(in)}}$ is the length of the outside (inside) region, and k_{H} and k_{p} are the wavenumbers of the Hawking and partner modes respectively, in units of ξ^{-1} . The integral is performed over the region in the correlation function bounded by $-L_{\text{out}}/\xi < x < 0$ and $0 < x' < L_{\text{in}}/\xi$. The zero-temperature static structure factor is given by $S_0 = (U_{k_{\text{H}}} + V_{k_{\text{H}}})(U_{k_{\text{p}}} + V_{k_{\text{p}}})$, where U_i and V_i are the Bogoliubov

¹Department of Physics, Technion – Israel Institute of Technology, Haifa, Israel. *e-mail: jeffs@physics.technion.ac.il

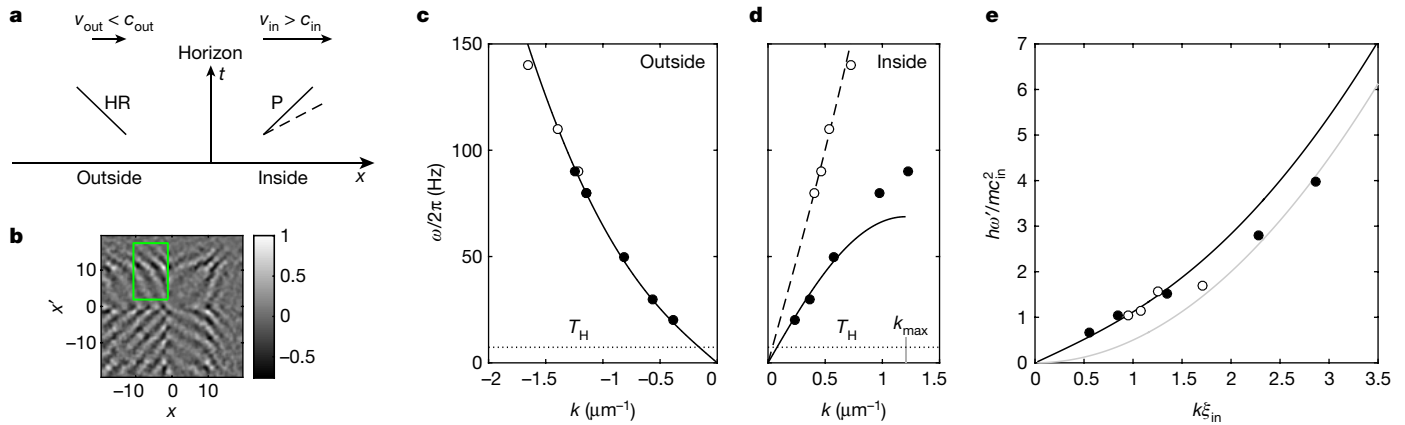


Fig. 1 | Hawking and partner modes. **a**, A space-time diagram showing the modes outgoing from the horizon. In addition to the Hawking mode (HR) and negative-energy partner mode (P) indicated by solid lines, the dashed line indicates the positive-energy mode that copropagates with the flow in the comoving frame. The partner and copropagating modes form a tilted sound cone inside the analogue black hole. The horizontal arrows indicate the flow of the condensate. **b**, The correlation function at 50 Hz from the oscillating horizon experiment (see Methods). **c**, **d**, Dispersion relations. Circles are measurements from the oscillating horizon experiment. The solid and dashed curves are fits of Bogoliubov

spectra, including a Doppler shift. The dotted lines indicate the Hawking temperature. **c** shows the dispersion relation outside the analogue black hole; **d** shows the dispersion relation inside the analogue black hole. The filled circles and solid curve indicate the partner mode and the open circles and dashed curve indicate the copropagating mode. k_{max} indicates the ultraviolet cut-off. **e**, The dispersion relation inside the analogue black hole, in the ‘free-falling’ comoving frame. The black curve is the Bogoliubov dispersion relation, and the grey curve is the parabolic dispersion relation of a free particle.

coefficients for the phonons, which are not related to the Bogoliubov coefficients introduced by Hawking. It is natural that S_0 appears in equation (2) given that the density amplitude of a phonon is proportional to $U_i + V_i$ (ref. ²⁵). The only assumption in equation (2) is that modes with different frequencies are uncorrelated²⁸. It is not necessary that the thermal population be zero. Furthermore, equation (2) is exact for a stationary configuration³³.

Here the analogue black hole is created in a Bose–Einstein condensate consisting of 8,000 ⁸⁷Rb atoms (see Methods). The elongated condensate is confined in a focused laser beam. The region $x < 0$ is illuminated with an additional laser beam that creates a positive potential, as illustrated in the inset to Fig. 2a. Thus, there is a downward potential step—a waterfall potential—near $x = 0$. The step potential moves at a constant speed of 0.16 mm s^{-1} , which is equivalent to the condensate flowing at constant speed in the reference frame in which the step is stationary. The condensate flows over the step, which accelerates the $x > 0$ part of the condensate to supersonic speeds. The correspondingly lower density and speed of sound are seen in Fig. 2a, b.

The Hawking radiation experiment is repeated 7,400 times, giving a density profile $n(x)$ for each run. The ensemble-averaged $n(x)$ is shown in Fig. 2a, where the circle indicates the location of the horizon. The speed of sound $c(x)$ can be derived from $n(x)$ by the relation (see Supplementary Information)

$$c(x) = \sqrt{\frac{2\hbar a \omega_r(x) n(x)}{m}} \sqrt{\frac{1 + 3n(x)a/2}{(1 + 2n(x)a)^{3/2}} - \frac{\hbar\omega_{r_0}}{2U_0}} \quad (3)$$

where a is the scattering length, $\omega_r(x)$ is the radial trapping frequency, and ω_{r_0} and U_0 are the radial trapping frequency and potential depth at the laser focus, respectively. Using equation (3), we obtain the ensemble-averaged $c(x)$ shown in Fig. 2b. Furthermore, $n(x)$ and $c(x)$ are computed for the average of each five adjacent runs. The predicted Hawking temperature is then computed using equation (1), indicated by the black curve in Fig. 2c, where each point on the curve corresponds to one set of five runs. The average over the black curve gives a predicted Hawking temperature of $0.351(4) \text{ nK}$, or $0.125(1) \times mc_{\text{out}}^2$, where the uncertainty reflects the uncertainty in the speed of sound and statistical uncertainty.

We compare the density fluctuations at a pair of points (x, x') in Fig. 2a over the ensemble of 7,400 runs. Figure 3a shows the resulting density–density correlation function for every pair of points. The dark

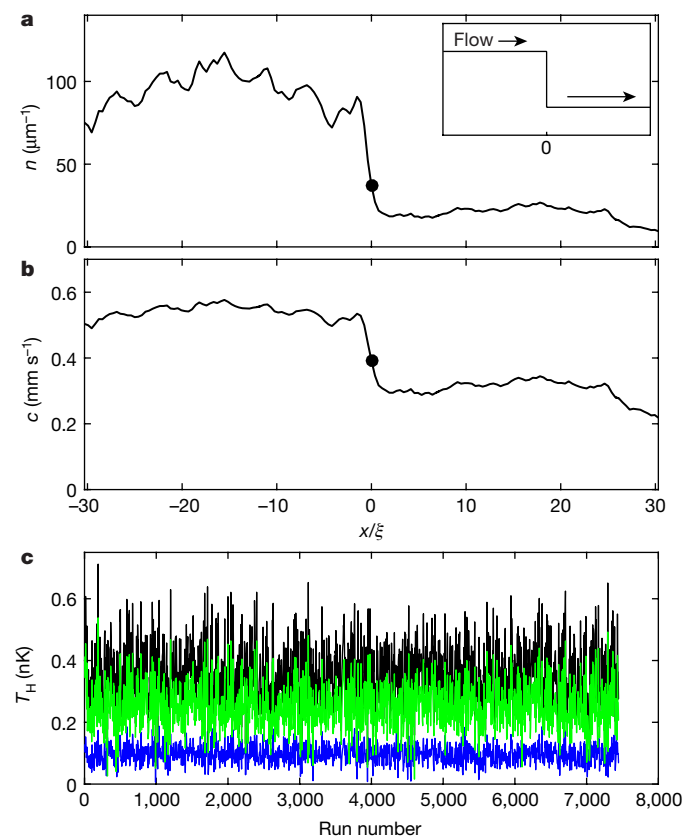


Fig. 2 | Profile of the analogue black hole. **a**, Density. The average of the 7,400 runs of the experiment is shown, where the circle indicates the horizon. Inset, schematic illustration of the step potential and the flow of the condensate; x axis as in main panel. **b**, The speed of sound by equation (3). **c**, The predicted Hawking temperature by equation (1). Each point is computed from the average of five runs of the experiment. The green and blue curves are the first and second terms in equation (1), respectively, and the black curve is the sum of the two terms, that is, the predicted Hawking temperature.

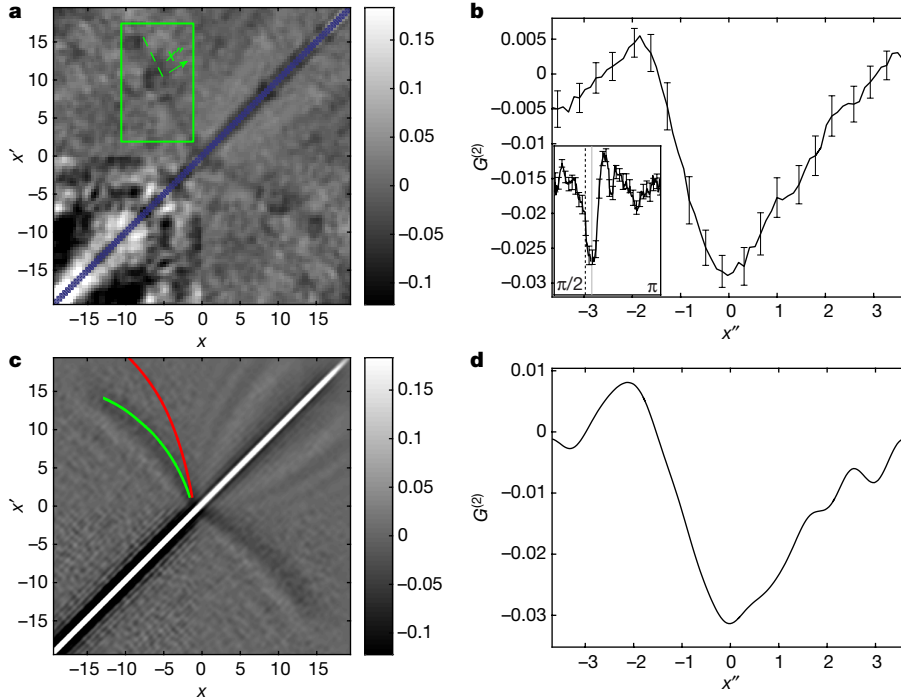


Fig. 3 | Measured Hawking radiation. **a**, The correlation function. The band extending from the origin represents the correlations between the Hawking and partner particles. The green rectangle is the area used for the two-dimensional Fourier transform. The dashed line indicates the hydrodynamic angle for Hawking–partner pairs. **b**, The profile of the correlation band along the x'' direction in **a**. Inset, the angular profile of **a**.

band extending from the centre of the figure represents the correlations between the Hawking and partner particles. Figure 3a is integrated along line segments at various angles, as shown in the inset of Fig. 3b. This angular profile gives the angle of the Hawking–partner correlation band, as indicated by the grey line. It can be seen that the correlation band is $5(1)^\circ$ from the hydrodynamic angle. The latter is derived under the assumption that the correlations propagate at the wave speeds $c_{\text{out}} - v_{\text{out}}$ and $v_{\text{in}} - c_{\text{in}}$ outside and inside the black hole, respectively. The profile of the band in the perpendicular x'' direction, averaged over the length of the band, is shown in Fig. 3b. Figure 3c, d shows a numerical simulation that employs a non-polynomial Gross–Pitaevskii equation and the truncated Wigner method¹¹, using parameters similar to the experiment. The results are similar to those in Fig. 3a, b. The maximum near $x'' = -2$ in Fig. 3b was also apparent in a previous numerical simulation¹⁴. The green curve in Fig. 3c shows the hydrodynamic path of Hawking and partner modes, which travel at $c(x) - v(x)$ and $v(x) - c(x)$ outside and inside the black hole, respectively. The red curve shows the Hawking and copropagating modes, where the latter propagate with speed $v(x) + c(x)$. It can be seen that the simulation is consistent with the Hawking–partner pairs (green curve), rather than the Hawking–copropagating pairs (red curve), as expected.

We extract the correlations between pairs of Hawking and partner modes by equation (2). The Fourier transform is performed in the region outlined in green in Fig. 3a. The resulting correlation pattern $S_0 |\langle \hat{b}_H \hat{b}_P \rangle|^2$ is shown in Fig. 4a. We obtain a one-dimensional plot of $S_0^2 |\langle \hat{b}_H \hat{b}_P \rangle|^2$ from the Fourier transform of the profile in Fig. 3b, by the following relation²⁸ derived from equation (2)

$$S_0 \langle \hat{b}_H \hat{b}_P \rangle = \sqrt{-\tan\theta - \cot\theta} \int dx'' e^{ikx''} G^{(2)}(x, x') \quad (4)$$

where θ is the angle of the correlation band in the $x-x'$ plane in Fig. 3a, measured relative to the positive x axis. The resulting correlation spectrum is shown in Fig. 4b. The spectrum becomes negligible near the ultraviolet cut-off k_{max} as predicted¹³. The main contributions to the error bars are the uncertainties in the speeds of sound. The uncertainty

The grey and dotted vertical lines indicate the angle of the Hawking correlation band and the hydrodynamic angle, respectively, relative to the positive x axis. The error bars indicate the standard error of the mean. **c**, **d**, Numerical truncated Wigner simulations of **a** and **b**. The green curve in **c** corresponds to Hawking–partner pairs, and the red curve corresponds to Hawking–copropagating pairs.

in the angle of the correlation band, the uncertainty due to the region chosen for the analysis and the statistical uncertainty are also included.

Using the standard dispersion relation shown in Fig. 1, we can express $|\beta|^2 = 1/(e^{\hbar\omega/k_B T_H} - 1)$ as a function of wavenumber, where T_H is the predicted Hawking temperature. The resulting spectrum $S_0^2 (|\beta|^2 + 1) |\beta|^2$ is indicated by the grey curve of Fig. 4b. The finite width of the grey curve reflects the uncertainties in the speeds of sound and the flow velocities. Very good agreement with the measured correlation spectrum of Hawking radiation can be seen, with no free parameters. We can quantify this agreement by assigning a temperature to the measured spectrum according to the area enclosed by the spectrum, which is proportional to T_H^3 . With the error bars shown, this yields $T_H^{\text{meas}} = 0.124(6) \times mc_{\text{out}}^2$, which differs from the prediction by $-1(5)\%$.

For a given frequency, the oscillating horizon experiment shown in Fig. 1 gives us k_{out} for the Hawking mode, and the corresponding value or values of k_{in} for the partner and/or copropagating modes, depending on the frequency. We indicate these measured pairs of modes ($k_{\text{out}}, k_{\text{in}}$) as circles in Fig. 4a. The green circles indicate the Hawking–partner modes, and the red circles indicate the Hawking–copropagating modes. The correlation pattern of the Hawking radiation (the grey region) lies along the green circles. Thus the correlations are observed to be composed of Hawking–partner pairs, as expected¹⁴. There are no correlations along the red circles, so no correlations between Hawking and copropagating modes are seen. We can see that the experiment operates in the regime of linear dispersion because most of the correlations lie along the linear low- k section of the green circles. This is also seen in Fig. 1c, d, where the Hawking temperature indicated by the dotted line is in the linear section of the dispersion relations.

This work gives quantitative confirmation of the temperature and thermality of Hawking radiation, as predicted in the literature for our system. It seems that the Hawking radiation is not strongly affected by dispersion or coupling to the mode directed towards the analogue black hole (greybody factors). The measurement made here is based on the correlations between the Hawking and partner modes.

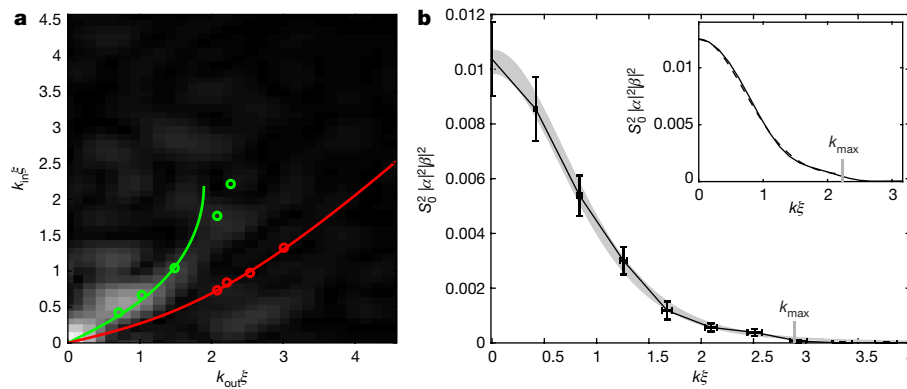


Fig. 4 | Spectrum of the Hawking radiation. **a**, The pattern of Hawking-partner correlations, computed within the green rectangle of Fig. 3a. The green circles and curve indicate the Hawking-partner modes, and the red circles and curve indicate the Hawking-copropagating modes, where the circles and curves are obtained from the oscillating horizon experiment. **b**, The correlation spectrum of the Hawking radiation. The black curve is the measured values; the Fourier transform of Fig. 3b. The error bars

These correlations are observed to be of the predicted magnitude, with no reduction caused by the underlying quantum (atomic) structure of the analogue black hole. For a real black hole, the Hawking temperature is an important link between Hawking radiation and black-hole thermodynamics, because it also arises from considerations of entropy. The thermality of Hawking radiation suggests that almost no information exits a real black hole, which is the basis of the information paradox.

Online content

Any methods, additional references, Nature Research reporting summaries, source data, statements of data availability and associated accession codes are available at <https://doi.org/10.1038/s41586-019-1241-0>.

Received: 16 September 2018; Accepted: 1 April 2019;

Published online 29 May 2019.

- Bekenstein, J. D. Black holes and entropy. *Phys. Rev. D* **7**, 2333–2346 (1973).
- Hawking, S. W. Black hole explosions? *Nature* **248**, 30–31 (1974).
- Hawking, S. W. Breakdown of predictability in gravitational collapse. *Phys. Rev. D* **14**, 2460–2473 (1976).
- Wald, R. M. On particle creation by black holes. *Commun. Math. Phys.* **45**, 9–34 (1975).
- Page, D. N. Particle emission rates from a black hole: massless particles from an uncharged, nonrotating hole. *Phys. Rev. D* **13**, 198–206 (1976).
- Visser, M. Thermality of the Hawking flux. *J. High Energy Phys.* [http://doi.org/10.1007/JHEP7\(2015\)009](http://doi.org/10.1007/JHEP7(2015)009) (2015).
- Unruh, W. G. Experimental black-hole evaporation? *Phys. Rev. Lett.* **46**, 1351–1353 (1981).
- Garay, L. J., Anglin, J. R., Cirac, J. I. & Zoller, P. Sonic analog of gravitational black holes in Bose–Einstein condensates. *Phys. Rev. Lett.* **85**, 4643–4647 (2000).
- Visser, M. Acoustic black holes: horizons, ergospheres and Hawking radiation. *Class. Quantum Gravity* **15**, 1767–1791 (1998).
- Balbinot, R., Fabbri, A., Fagnocchi, S., Recati, A. & Carusotto, I. Nonlocal density correlations as a signature of Hawking radiation from acoustic black holes. *Phys. Rev. A* **78**, 021603 (2008).
- Carusotto, I., Fagnocchi, S., Recati, A., Balbinot, R. & Fabbri, A. Numerical observation of Hawking radiation from acoustic black holes in atomic Bose–Einstein condensates. *New J. Phys.* **10**, 103001 (2008).
- Macher, J. & Parentani, R. Black-hole radiation in Bose–Einstein condensates. *Phys. Rev. A* **80**, 043601 (2009).
- Larré, P.-É., Recati, A., Carusotto, I. & Pavloff, N. Quantum fluctuations around black hole horizons in Bose–Einstein condensates. *Phys. Rev. A* **85**, 013621 (2012).
- Recati, A., Pavloff, N. & Carusotto, I. Bogoliubov theory of acoustic Hawking radiation in Bose–Einstein condensates. *Phys. Rev. A* **80**, 043603 (2009).
- Steinhauer, J. Measuring the entanglement of analogue Hawking radiation by the density–density correlation function. *Phys. Rev. D* **92**, 024043 (2015).
- Jacobson, T. A. & Volovik, G. E. Event horizons and ergoregions in ^3He . *Phys. Rev. D* **58**, 064021 (1998).
- Schützhold, R. & Unruh, W. G. Hawking radiation in an electromagnetic waveguide? *Phys. Rev. Lett.* **95**, 031301 (2005).
- de Nova, J. R. M., Guéry-Odelin, D., Sols, F. & Zapata, I. Birth of a quasi-stationary black hole in an outcoupled Bose–Einstein condensate. *New J. Phys.* **16**, 123033 (2014).

include the standard error of the mean and systematic errors. The grey curve is the predicted thermal spectrum using the Hawking temperature from equation (1). The uncertainty is indicated by the width of the curve. Inset, the correlation spectrum from the numerical simulation. The solid curve is the Fourier transform of Fig. 3d, and the dashed curve is the predicted thermal spectrum from equation (1).

- Weinfurter, S., Tedford, E. W., Penrice, M. C. J., Unruh, W. G. & Lawrence, G. A. Measurement of stimulated Hawking emission in an analogue system. *Phys. Rev. Lett.* **106**, 021302 (2011).
- Rousseaux, G., Mathis, C., Maïssa, P., Philbin, T. G. & Leonhardt, U. Observation of negative-frequency waves in a water tank: a classical analogue to the Hawking effect? *New J. Phys.* **10**, 053015 (2008).
- Euvé, L.-P., Michel, F., Parentani, R., Philbin, T. G. & Rousseaux, G. Observation of noise correlated by the Hawking effect in a water tank. *Phys. Rev. Lett.* **117**, 121301 (2016).
- Philbin, T. G. et al. Fiber-optical analog of the event horizon. *Science* **319**, 1367–1370 (2008).
- Nguyen, H. S. et al. Acoustic black hole in a stationary hydrodynamic flow of microcavity polaritons. *Phys. Rev. Lett.* **114**, 036402 (2015).
- Lahav, O. et al. Realization of a sonic black hole analog in a Bose–Einstein condensate. *Phys. Rev. Lett.* **105**, 240401 (2010).
- Shammass, I., Rinott, S., Berkovitz, A., Schley, R. & Steinhauer, J. Phonon dispersion relation of an atomic Bose–Einstein condensate. *Phys. Rev. Lett.* **109**, 195301 (2012).
- Schley, R. et al. Planck distribution of phonons in a Bose–Einstein condensate. *Phys. Rev. Lett.* **111**, 055301 (2013).
- Steinhauer, J. Observation of self-amplifying Hawking radiation in an analogue black-hole laser. *Nat. Phys.* **10**, 864–869 (2014).
- Steinhauer, J. Observation of quantum Hawking radiation and its entanglement in an analogue black hole. *Nat. Phys.* **12**, 959–965 (2016).
- Michel, F., Coupechoux, J.-F. & Parentani, R. Phonon spectrum and correlations in a transonic flow of an atomic Bose gas. *Phys. Rev. D* **94**, 084027 (2016).
- Coutant, A. & Weinfurter, S. Low-frequency analogue Hawking radiation: the Bogoliubov–de Gennes model. *Phys. Rev. D* **97**, 025006 (2018).
- Fabbri, A. & Pavloff, N. Momentum correlations as signature of sonic Hawking radiation in Bose–Einstein condensates. *SciPost Phys.* **4**, 019 (2018).
- Carusotto, I. & Balbinot, R. Acoustic Hawking radiation. *Nat. Phys.* **12**, 897–898 (2016).
- Robertson, S., Michel, F. & Parentani, R. Assessing degrees of entanglement of phonon states in atomic Bose gases through the measurement of commuting observables. *Phys. Rev. D* **96**, 045012 (2017).

Acknowledgements We thank the participants of the LITP Analogue Gravity Workshop for their conversations. We thank I. Carusotto, R. Parentani, D. Marolf and F. Michel for comments. This work was supported by the Israel Science Foundation.

Author contributions J.R.M.d.N. and J.S. designed and built the experimental apparatus. J.R.M.d.N., K.G. and V.I.K. performed theoretical calculations. J.S. acquired the data. K.G., V.I.K. and J.S. analysed the data. J.R.M.d.N. performed the numerical simulations. J.R.M.d.N. and J.S. wrote the manuscript with input from all authors.

Competing interests The authors declare no competing interests.

Additional information

Supplementary information is available for this paper at <https://doi.org/10.1038/s41586-019-1241-0>.

Reprints and permissions information is available at <http://www.nature.com/reprints>.

Correspondence and requests for materials should be addressed to J.S.

Publisher's note: Springer Nature remains neutral with regard to jurisdictional claims in published maps and institutional affiliations.

© The Author(s), under exclusive licence to Springer Nature Limited 2019

METHODS

Laser beam potentials. The focused laser beam trap is red-detuned to create an attractive potential, with wavelength 812 nm and waist 3.9 μm . We measure its transverse trapping frequency by applying a short pulse of a magnetic field gradient, which excites a dipole oscillation. We observe the oscillations as a function of time, giving a trapping frequency of 130 Hz at the focus of the laser. The laser beam that creates the positive potential step is blue-detuned with wavelength 442 nm.

Improvements to the experimental setup. The experimental apparatus is as described previously²⁸, with improvements. One such improvement is a magnetic field environment with lower noise, as a result of improved power supplies which activate four of the six sets of magnetic field coils. This is important because static magnetic field gradients apply forces to the condensate via the Zeeman shift. Since the condensate is decompressed and weakly trapped in the axial direction, it is very sensitive to such gradients. In addition, five out of each 200 runs serve as reference images. For these images the step potential is not applied and the power of the focused laser trap is reduced, which further increases the sensitivity to an axial magnetic field gradient or to a tilt resulting in a gravitational gradient. The axial centre of the reference images is found, and any axial shift is corrected by a slight fractional adjustment ($\leq 3 \times 10^{-4}$) of the current in one of the axial magnetic field coils. In addition, the optics has been improved, with reduced aberrations. This includes the optics for creating and translating the waterfall potential, as well as for imaging. Specifically, the system of lenses has been redesigned, and the acousto-optic modulator used to translate the waterfall potential has been replaced by a rotating mirror. Furthermore, there is improved mechanical stability in the magnetic field coils and optics. In addition, the temperature of the room has improved long-term stability.

Speed of sound calculation. The first factor in equation (3) is the usual expression for a quasi-one-dimensional condensate with harmonic radial confinement. The second factor reduces the speed of sound owing to the transverse degree of freedom. The first term in the square root in the second factor accounts for the finite density³⁴. The second term accounts for the finite depth of the potential.

Correlation function filtering. Figure 3a has been filtered to remove the effects of imaging shot noise, imaging fringes, and overall slopes. The background of Fig. 3b was found by a fit of a Gaussian plus a constant background, and has been removed. The simulation has also been filtered and its constant background removed.

Oscillating horizon experiment. We measure the predicted Hawking temperature, as well as the correlation spectrum of Hawking radiation as a function of wave-

number. To compare the two measurements we use the relation between frequency and wavenumber, that is, the dispersion relation, which is readily measured by the oscillating horizon technique we introduced in previous work²⁸. Waves are generated by causing the position of the step potential to oscillate with a definite frequency and an amplitude of 0.5 μm . This oscillation at the horizon creates outgoing waves outside and inside the analogue black hole. The experiment is repeated 70 to 429 times with a given frequency and a random phase each run. The correlation function is computed, as shown in Fig. 1b. The wavenumbers are found by computing the Fourier transform within the green rectangle, the same region where Hawking radiation is observed in Fig. 3a. In this region, the horizontal and vertical directions correspond to outside and inside, respectively. The resulting dispersion relations are shown in Fig. 1c, d. The curves are fits of Bogoliubov dispersion relations including a Doppler shift, yielding $c_{\text{out}} = 0.519(6) \text{ mm s}^{-1}$, $v_{\text{out}} = 0.229(4) \text{ mm s}^{-1}$, $c_{\text{in}} = 0.31(2) \text{ mm s}^{-1}$ and $v_{\text{in}} = 0.90(1) \text{ mm s}^{-1}$. The fit to the lower points misses the two highest points of the negative-energy (partner) branch of the dispersion relation in Fig. 1d. We can see the discrepancy more clearly by considering the frame that is comoving with the fluid inside the analogue black hole, in which waves travelling to the left and right have the same dispersion relation, as seen in Fig. 1e. For larger k , the measured points are not consistent with a spectrum of the Bogoliubov form. The outlying points in Fig. 1d are probably due to off-resonance stimulation of the excitations near k_{max} . The modes in the radial direction^{35,36} should play no part because their effect is much smaller and occurs at much higher frequency than seen here²⁵. Furthermore, there may be weak excitation of the low-lying copropagating modes along the dashed curve of Fig. 1d, but they are not resolved from the partner modes along the solid curve. These effects are in agreement with our theoretical model of the oscillating horizon experiment (see Supplementary Information).

Data availability

The data that support the plots within this paper and other findings of this study are available from the corresponding author upon reasonable request.

34. Salasnich, L., Parola, A. & Reatto, L. Dimensional reduction in Bose–Einstein-condensed alkali-metal vapors. *Phys. Rev. A* **69**, 045601 (2004).
35. Steinhauer, J. et al. Bragg spectroscopy of the multibranch Bogoliubov spectrum of elongated Bose–Einstein condensates. *Phys. Rev. Lett.* **90**, 060404 (2003).
36. Tozzo, C. & Dalfovo, F. Bogoliubov spectrum and Bragg spectroscopy of elongated Bose–Einstein condensates. *New J. Phys.* **5**, 54 (2003).